C. Bailly, B. André, T. Castelain
(Université de Lyon)
C. Henry, G. Bodard
(Snecma)
M. Porta
(Airbus)

E-mail: christophe.bailly@ec-lyon.fr

DOI : 10.12762/2014.AL07-06

An analysis of shock noise components

Screech and broadband shock-associated noise linked to the presence of a shock-cell structure in supersonic jets are reviewed in this paper. Only underexpanded supersonic circular jets issued from a convergent nozzle are considered here. An overview of the flow and of these two noise components is presented, based on recent experimental and numerical work. Flight effects on broadband shock-associated noise are also introduced, within the framework of aeronautical applications.

Introduction

The purpose of this introductory paper is to provide an overview of shock noise generated by underexpanded supersonic jets. This additional component to the mixing noise produced by turbulence is associated with the presence of a shock-cell structure in the jet supersonic core. Shock noise is composed of screech tones and a broadband shock-associated noise (BBSAN). Flight effects on the BBSAN are also discussed, within the context of aeronautical applications. The secondary stream of commercial engines is indeed underexpanded during the climb and cruise phases of a flight. While BBSAN comes alongside screech in model laboratory jets, the latter is not observed on civil aircraft engines, since the nozzle is not axisymmetric. Screech is however known to have a strong impact on the turbulent jet dynamics. Screech suppression is therefore an essential effort for studying BBSAN. This analysis of shock noise components is also based on recent experimental and numerical work carried out by the authors. Several methods have been successfully implemented to characterize the jet flow and its acoustic field: high-speed Schlieren technique, crossed Schlieren apparatus, static pressure measurements and velocimetry (LDV, PIV), as well as acoustic measurements. A statistical modelling of BBSAN using a steady solution of averaged Navier-Stokes equations is also assessed.

The paper is organized as follows. A brief description of underexpanded jets is first given. An analysis of Screech and BBSAN is then proposed. Flight effects on BBSAN are finally discussed and concluding remarks are drawn.

Underexpanded supersonic jets

A jet issuing from a converging nozzle is sonic for a nozzle pressure ratio greater than a critical value, where the nozzle pressure ratio (NPR) is defined as the reservoir or stagnation pressure p_t divided by the ambient pressure p_∞, $\mathrm{NPR} \equiv p_t / p_\infty$. For an air flow, this critical value is given by $[(\gamma+1)/2]^{\gamma/(\gamma-1)} \simeq 1.89$, where γ is the specific heat ratio.

A perfectly expanded jet, that is, a shock-free jet, is then obtained for this particular value since the exit pressure p_e is equal to the ambient pressure p_∞, noting also that a converging nozzle is characterized by a design Mach number M_d equal to unity at the nozzle exit.

For higher values of NPR, the Mach number at the nozzle exit is still equal to unity, but the exit pressure p_e no longer matches the ambient pressure p_∞. As a result, a weak shock-cell structure appears inside the transonic jet jet to adapt the jet pressure field to this ambient pressure and the jet is said to be underexpanded, since $p_e > p_\infty$. The fully expanded jet Mach number M_j defined by

$$M_j = \sqrt{\frac{2}{\gamma-1}\left(\mathrm{NPR}^{\frac{\gamma-1}{\gamma}} - 1\right)} \qquad (1)$$

is also often used to define the jet operating point. This Mach number corresponds to the design Mach number M_d of a convergent-divergent nozzle, which should be considered to obtain a shock-free jet at this given NPR.

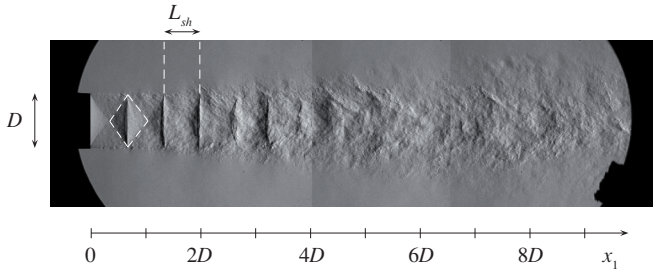

Figure 1 - Spark Schlieren visualization (conventional Z-type system, 4 μs time exposure) of an underexpanded jet at $M_j = 1.15$ and stagnation temperature $T_t = T_\infty$, issued from a notched (to avoid screech, see André et al. [6]) convergent nozzle of diameter D. The Reynolds number is $Re_D = u_j D/\nu = 1.27\times10^6$. Longitudinal density gradients are visualized here thanks to the orientation of the knife-edge, light and dark regions corresponding respectively to expansion and compression regions for the flow in shock cell diamond patterns [5].

As an illustration, an instantaneous view of a supersonic jet at M_j=1.15 is shown in figure 1. The quasi-periodic diamond pattern associated with expansion and compression waves trapped inside the jet plume is clearly visible from the nozzle exit, as well as the developing turbulent flow. The NPR is not high enough to observe a Mach disk inside the first shock cell in this case [1], but it can be seen at $M_j = 1.5$, for instance [5]. Various experimental techniques can be used to obtain an accurate picture of the jet flow development [7]. The longitudinal and transverse mean velocity components of the underexpanded jet at $M_j = 1.10$ obtained from particle image velocimetry, are displayed in figure 2. The axial mean velocity increases during expansion stages, which occur within light right-pointing triangles of the Schlieren view shown in figure 1, and decreases during compression stages associated with dark left-pointing triangles. It thus reaches a maximum corresponding to axial edges of shock-cell diamond patterns. Expansion and compression zones are also clearly identifiable by looking at the mean transverse velocity.

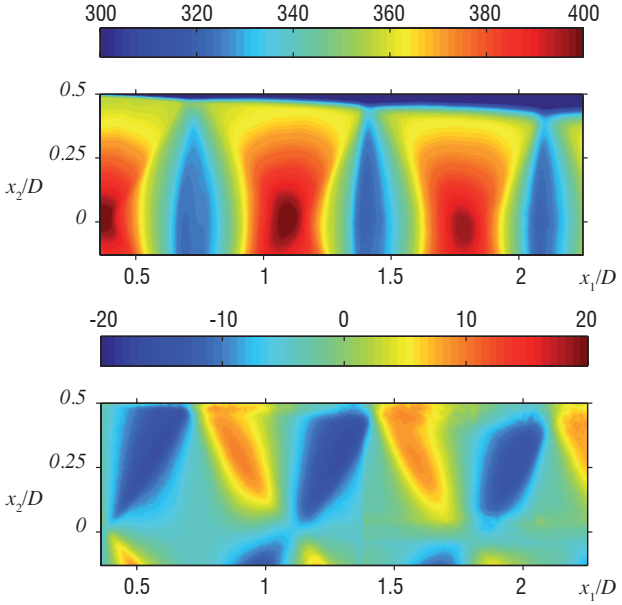

Figure 2 - Measured longitudinal (top) and transverse (bottom) mean velocity field (color scale in m.s^{-1}) in a plane containing the jet axis for M_j = 1.15, with a notched convergent nozzle and an additional slow coflow at $M_f = 0.05$ to ensure seeding of the supersonic jet surroundings. The PIV set-up leads to about 190 velocity vectors over one jet diameter. More details regarding the quality checks can be found in André [5,10].

The quasi-periodic shock-cell structure can be approximated by a vortex sheet model first introduced by Prandtl (1904) and modified by Pack (1950), as discussed in the review by Powell [28]. The corresponding axisymmetric pressure disturbance $p_s(x_1, x_\perp)$, where $x_\perp = (x_2^2 + x_3^2)^{1/2}$

$$p_{sh} / p_\infty = \sum_{n=1}^{\infty} A_n \phi_n(x_\perp) \cos(k_n x_1) \qquad (2)$$

is obtained as the solution of the Euler equations, linearized around a perfectly expanded supersonic jet, assuming that $p_e - p_\infty$ remains small. The complete expression for the amplitude A_n, the radial distribution of each mode ϕ_n and its wave number k_n can be found in Tam *et al.* [32,33]. One useful result of this simple model is the estimation of the shock-cell length, given by

$$L_{sh} \simeq 2\pi / k_1 \simeq 1.306 \beta D_j \qquad (3)$$

where D_j is the fully expanded jet diameter at M_j and the parameter β is defined as $\beta = (M_j^2 - 1)^{1/2}$. For weakly imperfectly expanded supersonic jets, it can been shown that $D_j / D = 1 + O(\beta^4)$. Therefore, the nozzle diameter D will be used as a reference length scale thereafter.

Narrow-band acoustic spectra measured in the far field for an underexpanded jet at $M_j = 1.10$ are plotted in figure 3, as a function of the Strouhal number $St = f D/u_j$, where $u_j = c_j M_j$ is the jet velocity defined from (1), and for different angular positions of the observer. There are three contributions to these spectra: mixing noise, screech and broadband shock-associated noise. Mixing noise is produced by jet flow turbulence and is the only component encountered in both subsonic and supersonic jets. It can thus be identified by continuation as M_j increases and forms the whole broadband part of the spectrum at $\theta = 30°$. This is discussed in detail by Bogey & Bailly [13] and the reader can refer to the review by Tam [34] for Mach waves. The tonal component and the subsequent harmonics are screech, indicated by arrows in figure 3, and broadband shock-associated noise (BBSAN), indicated by the dashed line, and corresponds to the broadband hump dominating mixing noise in the upstream direction. These last two components are linked to the presence of a shock-cell structure in the jet. At this stage, it is important to observe the high amplitude of screech, with an emergence of the fundamental peak of about 30 dB at $\theta = 130°$. While BBSAN comes alongside screech in model laboratory jets, the latter does not seem to be observed on civil aircraft engines. Screech is however known to have a strong impact on the turbulent jet dynamics [29], leading to a completely different jet development. Screech suppression is therefore essential for BBSAN study [6].

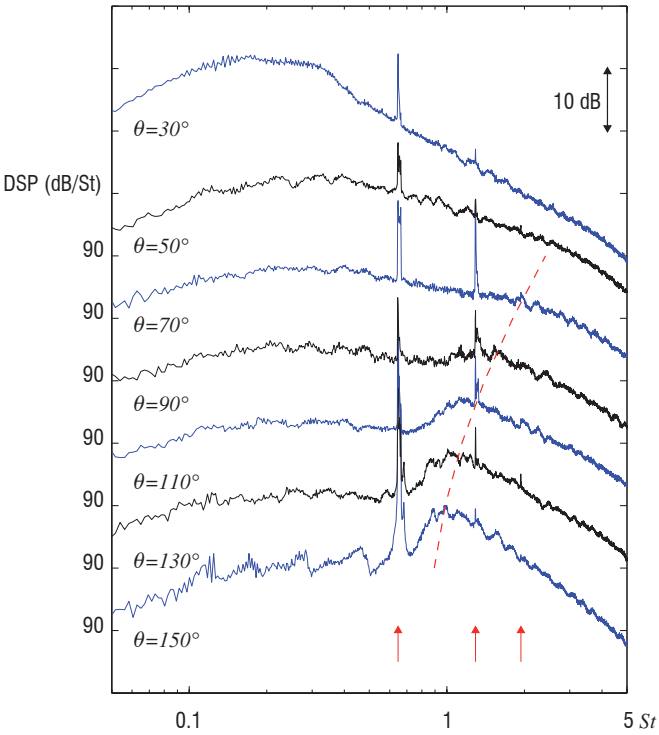

Figure 3 - Narrow-band acoustic spectra of M_j = 1.10 jet, measured at r/D = 53.2 as a function of the Strouhal number St, and for different angular positions. The angle θ is taken from the downstream jet axis. The red dashed line corresponds to relation (7) and the red arrows indicate the fundamental screech frequency and its two first harmonics. Data from André [5].

Screech

Screech is described as a feedback mechanism along the mixing layer of the jet, as studied at length by Powell [25–27] since the fifties for rectangular and round choked jets. Vortical structures are generated at the nozzle lip, and are convected downstream in the mixing layer. These perturbations interact with shock-cells and create acoustic waves that propagate upstream to the nozzle lip in the ambient medium and then trigger subsequent instability waves, which form new vortical structures along the shear layer bounding the jet. A simple acoustic model can be derived to explain the frequency selection. The pressure field resulting from a phased array of acoustic monopole sources by considering the axisymmetric mode as an illustration, each fixed source being located at the end of a shock-cell with a phase shift determined by the convection velocity, can be written as [22,30]

$$p(r,\theta,t) = \exp\left[\frac{i2\pi(c_\infty t - r)}{\lambda_s}\right] \times \sum_j \frac{S_j}{r_j} \exp\left[-i2\pi j \frac{L_{sh}}{\lambda_s}\left(\frac{1}{M_c} - \cos\theta\right)\right] \quad (4)$$

The observer position (r, θ) from the nozzle exit is assumed to be in the far field, the source to observer distance and strength of the j-th source are r_j and S_j, λ_s is the acoustic wavelength, $M_c = u_c / c_\infty$ is the convective Mach number and c_∞ the ambient speed of sound. The mechanism is sustained only if all of the acoustic waves reach the nozzle lip in phase, that is

$$\frac{L_{sh}}{\lambda_s}\left(\frac{1}{M_c} + 1\right) = n \quad \text{or} \quad \frac{n}{f_s} = \frac{L_{sh}}{u_c} + \frac{L_{sh}}{c_\infty} \quad (5)$$

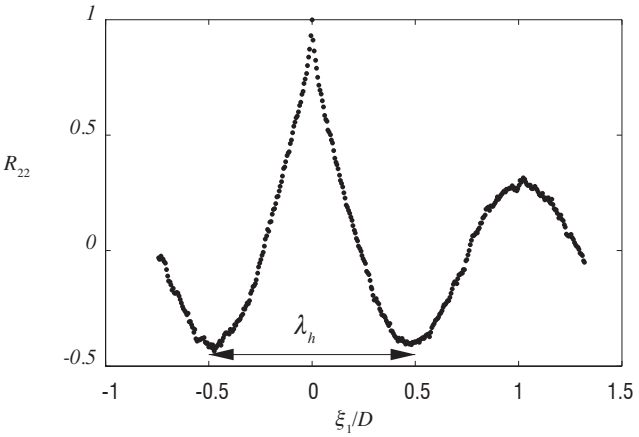

Figure 4 - Correlation function R_{22} measured by PIV at $x_1 = 3D$ along the lip line ($x_\perp = D/2$) for a screeching $M_j = 1.10$ jet, as a function of the axial separation ξ_1 normalized by the nozzle diameter. The length wave $\lambda_h = u_c / f_s \simeq D$ can be identified with $u_c = 0.65 u_j$ and $f_s = 5870$ Hz.

The sum of the convection time of vortical structures along the shear layer plus the acoustical return time to the nozzle lip is an integer of the screech oscillation periods. Using the value $u_c = 0.65 u_j$ indirectly measured [6], the Strouhal number associated with the fundamental mode $n = 1$ for the $M_j = 1.10$ jet is $St_s \cong 0.65$, in good agreement with experiments reported in figure 3. The screech frequency does not vary with the angular observer position. The directivity

$$D(\theta) = \lim_{r\to\infty} r^2 \overline{p'^2} / (\rho_\infty c_\infty^2)^2$$

of the phased array sources (4) presents a maximum in the upstream direction for this frequency. The simplicity of expression (5) should not hide the complexity of the physics involved. The structure of low-frequency instability waves and of the acoustic field can indeed take different modal forms [2, 27, 29, 30]. Screech for the $M_j = 1.1$ jet corresponds to the axisymmetric mode A_1, for instance.

Identification of shock-cells contributing to screech can be conducted through the examination of correlation functions among other quantities. The following two-point velocity correlation function,

$$R_{22}(\boldsymbol{x},\xi) = \frac{\overline{u'_2(\boldsymbol{x},t)\, u'_2(\boldsymbol{x}+\xi,t)}}{\overline{u'^2_2(\boldsymbol{x})}\ \overline{u'^2_{2'}(\boldsymbol{x}+\xi)}} \quad (6)$$

is shown in figure 4, as a function of the longitudinal separation coordinate $\xi = (\xi_1, 0, 0)$, and for a reference point x along the lip line. The wavelength $\lambda_h = u_c / f_s$ associated with Powell's model (5) can be clearly identified. By examining R_{22} and the integral length scale, a particular behavior can be identified along the five first shock cells for the $M_j = 1.10$ jet, which could suggest that these cells are involved in the screech generation [5,23,24,31].

Broadband shock-associated noise

As mentioned previously, screech must be suppressed in small-scale studies. This tonal noise can be removed by means of a notched nozzle [6] in a less intrusive manner than by introducing a protrusion or tab on the nozzle lip [8] in a laboratory facility. Harper-Bourne & Fisher [14] were the first to model BBSAN by a phased array of monopole sources similar to (4). The far-field results from the interference of these sources, with a peak frequency for the hump given by

$$f_p = \frac{u_c}{\bar{L}_{sh}(1 - M_c \cos\theta)} \quad (7)$$

This relation is in agreement with experimental observations reported in figure (3), by adjusting the value of the mean shock-cell spacing $\bar{L}_{sh}$. Harper-Bourne & Fisher also noticed that over a wide range of β, the BBSAN intensity varies as $I \propto (M_j^2 - 1)^2$ for convergent nozzles. Another approach was developed later by Tam *et al.* [32,34], considering the interaction of instability waves $u_t \sim e^{i(\alpha x - \omega t)}$ where $\alpha \simeq \omega / u_c$, with the shock-cell structure (2), that is, $u_{sh} \sim \cos(k_{sh} x)$ with $k_{sh} = 2\pi / L_{sh}$. Perturbations are given by their product

$$u_t u_{sh} \sim \underbrace{e^{i[(\alpha - k_{sh})x - \omega t]}}_{W^-} + \underbrace{e^{i[(\alpha + k_{sh})x - \omega t]}}_{W^+} \quad (8)$$

The phase velocity of waves W^- is $v_\varphi^- = \omega / (\alpha - k_{sh})$. For values of k_{sh} slightly greater than α, this phase velocity is negative and can be greater than the ambient speed of sound c_∞. Mach waves are then generated in the upstream direction, as illustrated in figure 5, with an emission angle such that $\cos\theta = c_\infty / v_\varphi^-$. Note that expression (7) is recovered from this condition. Regarding waves W^+, the phase velocity can be written as $v_\varphi^+ = \omega / (\alpha + k_{sh}) = u_c \omega / (\omega + k_{sh} u_c)$ and is thus always smaller than the convection velocity u_c. For the jet conditions considered here, u_c and thus v_φ^+ remain subsonic. Moreover, Tam & Tanna [32] found that for a convergent-divergent nozzle of design Mach number M_d, the acoustic intensity of BBSAN is proportional to $I \propto (M_j^2 - M_d^2)^2$. This expression is compatible with

Harper-Bourne & Fisher's result for convergent nozzles, for which $M_d = 1$. Note also that expression (3) still holds for a convergent-divergent nozzle. Interaction between convected turbulence and the shock-cell structure is also experimentally investigated in Pao & Seiner [24], and a critical review of the previous models is provided.

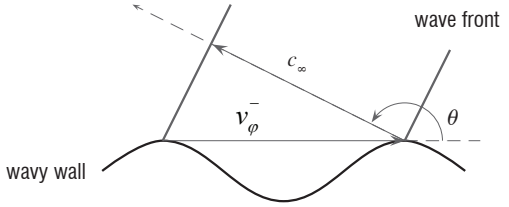

Figure 5 - Generation of Mach waves by a wavy wall moving at supersonic phase speed u_c, the direction of the radiation $\cos\theta = c_\infty / v_\varphi^-$ is obtained by matching the velocity trace along the flow direction. There is an analogy with the acoustic radiation of a vibrating plate for the reader familiar with vibroacoustics.

Morris & Miller [20] have developed a numerical model to predict BBSAN, in extending what has been done for mixing noise within the framework of statistical modelling [11, 21]. The inputs of such models are provided by a Reynolds-Averaged Navier-Stokes (RANS) solution. As a starting point, flow variables are split up among four contributions associated with the mean flow, the turbulent flow, the shock-cell structure and the fluctuations generated by the interaction between shocks and turbulence, including acoustic perturbations. For instance, the pressure term written as $\pi = (1/\gamma)\ln(p/p_\infty)$, is decomposed respectively into $\pi = \overline{\pi} + \pi_t + \pi_{sh} + \pi'$, where only π' is assumed to be unknown. For an isentropic flow, it can be shown that at the leading order, fluid dynamics equations can be reduced to the Euler equations linearized around the mean flow $(\overline{\pi}, \overline{\boldsymbol{u}})$, denoted hereafter by $\overline{\mathcal{L}}_i$ for $i = 0$ to 3. One has $\overline{\mathcal{L}}_0(\pi', \boldsymbol{u}') = 0$ for the energy equation written for the pressure variable here, and $\overline{\mathcal{L}}_i(\pi', \boldsymbol{u}') = f_i$ for the momentum equation ($i = 1$ to 3). The main source term for shock noise is given by $f = -\boldsymbol{u}_{sh} \bullet \nabla \boldsymbol{u}_t - \boldsymbol{u}_t \bullet \nabla \boldsymbol{u}_{sh}$ and corresponds to the source term already identified by Tam [34] for the interaction between turbulence and shocks. A vectorial Green function technique is introduced by Morris & Miller to solve this inhomogeneous linear system. The Green functions $(\Pi^n, \boldsymbol{V}^n)$, with $0 \le n \le 3$ linked to the number of scalar equations, must satisfy

$$\overline{\mathcal{L}}_i(\Pi^n, \boldsymbol{V}^n) = \delta(\boldsymbol{x} - \boldsymbol{y})\delta(t - \tau)\delta_{in} \tag{9}$$

for $i = 0, \ldots, 3$. Since there is no source term in the first equation for pressure ($i = 0$), one has $\Pi^0 \equiv 0$ and $V_i^0 \equiv 0$. The fluctuating pressure $p' = \rho_\infty c_\infty^2 \pi'$ is then directly related to the source term through the following integral

$$\pi'(x,t) = \sum_{n=1}^{3} \iint \Pi^n(\boldsymbol{x}, t; \boldsymbol{y}, \tau) f_n(\boldsymbol{y}, \tau) d\boldsymbol{y} d\tau \tag{10}$$

Assuming that the Π_n functions are known, this point is discussed in the next section, the pressure autocorrelation function $R_{pp}(\boldsymbol{x}, \tau)$, as well as the power spectral density $S_{pp}(\boldsymbol{x}, \omega)$, can be calculated under the assumption of an isotropic turbulence. The source term f is approximated by noting that $(\boldsymbol{u}_{sh})_i \sim \overline{u}_i \pi_{sh}$ and $\pi_{sh} = \rho_\infty c_\infty^2 p_{sh}$ and by assuming a local isotropy. In the end, $f_i(\boldsymbol{y}, \tau) = p_{sh}(\boldsymbol{y}) u_t(\boldsymbol{y}, \tau) / (\rho_\infty c_\infty l(\boldsymbol{y}))$, where $l(\mathbf{y})$ is a turbulent characteristic length scale. The final expression [16, 20] involves local turbulent characteristic scales, which are estimated from a RANS simulation. The static pressure p_{sh} associated with the shock-cell structure is also directly provided by the numerical solution.

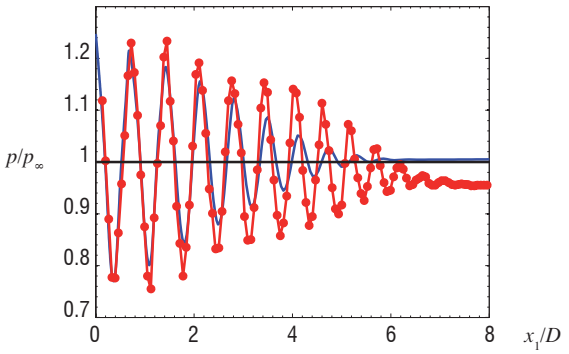

Figure 6 - Mean axial static pressure of the $M_j = 1.15$ jet normalized by p_∞, — RANS calculation [15], —•— measurements [7].

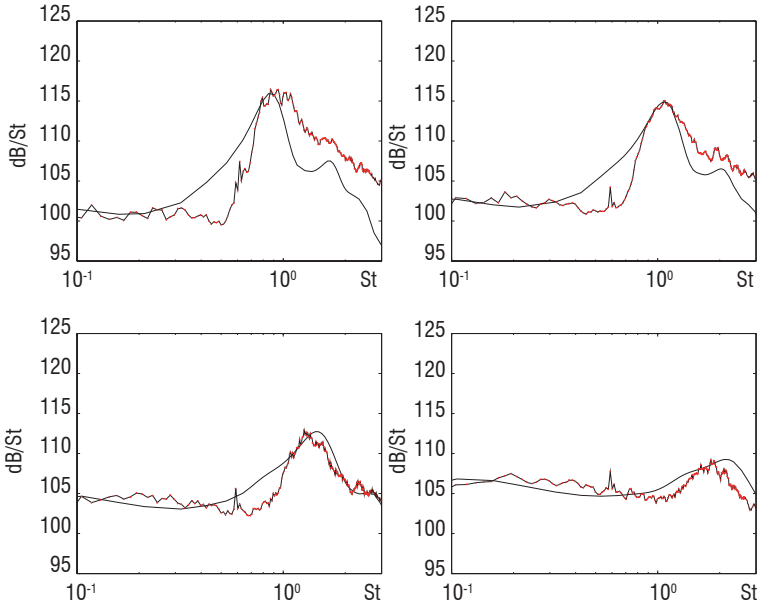

Figure 7 - Acoustic spectra in dB/St as a function of the Strouhal number $\mathrm{St} = fD/u_j$, of the $M_j = 1.15$ jet for an observer angle $\theta = 130°, 110°, 90°$ and $70°$; — measurements [5], — predicted BBSAN component [15], which is expected to dominate in the rear quadrant. The observer angle θ is taken from the downstream jet axis.

As an illustration, the computed mean axial static pressure is shown in figure 6 for the $M_j = 1.15$ jet, and is compared to measurements [5, 7]. The RANS calculations were done with the elsA CFD solver developed by Onera. A spatial Roe scheme was used and turbulence was modeled using the $k-\omega-SST$ model. The mesh contains approximately 150000 nodes with about 30 points in the first shock-cells in the axial direction and 20 points in the mixing layer for the radial direction. The shock locations are correctly predicted by the simulation and the overall agreement is quite satisfactory, though the shock damping is overestimated. The difference between calculations and experimental data for $x/D \geq 6$, where the flow becomes subsonic, stems from the pressure probe, which is designed to work at supersonic Mach numbers. The BBSAN component predicted by the statistical model is plotted in figure 7, as well as experimental results. The peak frequency f_p is correctly captured numerically and the emergence of BBSAN increases in the inlet direction ($\theta \to \pi$), as predicted by expression (7). The model is not expected to account for mixing noise and the good agreement observed at low frequencies ($\mathrm{St} \leq 0.5$) is rather a coincidence. Finally, this model makes BBSAN source distribution easy to study, through the examination of the integrand providing $S_{pp}(\boldsymbol{x}, \omega)$ at a given frequency. Close to the peak frequency f_p, sources are found to be widely spread along the shock-cell boundary in the mixing layer.

Flight effects on the BBSAN

The motivation for studying flight effects on the BBSAN is of course linked to aeronautical applications [17], as already mentioned in introduction. Figure 8 (top) illustrates the case of a dual-stream engine with a high bypass ratio. The central plug, the primary hot jet and the secondary cold and supersonic underexpanded jet can be identified. A RANS solution of a generic configuration is also shown. The shock-cell structure is confined between two shear layers [36], namely the inner shear layer between the primary and secondary stream and the outer layer between the secondary and the external stream.

It is not easy to reproduce this geometry in an anechoic wind tunnel, with a flight Mach number such as $0.8 \leq M_f \leq 0.9$. Moreover, amore basic configuration permits the role of key parameters to be better clarified. In this study, it has been chosen to set an underexpanded jet in the potential core of a larger subsonic jet to reproduce flight effects. As illustrated in Figure 8 (bottom), there is only one shear layer. The case of a free round underexpanded jet is thus recovered when the flight Mach number M_f goes to zero.

By referring to the work by Seiner [30], Tam [34] and Morris & Miller [20], the BBSAN source term is expected to be directly linked to the shock-cell strength and turbulence intensity, since BBSAN source term is proportional to pshut . From Schlieren visualizations and PIV data [5,9], the strength of the first shock cells, calculated as $(p_{max} - p_{min})/p_{min}$ inside each shock cell, has been consistently observed to become reduced in flight as M_f is increased. Moreover, an impressive expansion of the cell structure is observed with more shock cells visible. The evolution of each shock-cell length is reported in figure 9 for different flight Mach numbers. Except for the first cell, the shock length increases as Mf increases, in agreement with the vortex sheet model developed by Morris [19]. The external boundary layer thickness could slightly modulate this result by controlling the flow conditions at the nozzle exit, see figure 8 (bottom), but it is not easy to investigate this issue experimentally. Moreover, BBSAN acoustic sources are expected to be located downstream, unlike screech sources.

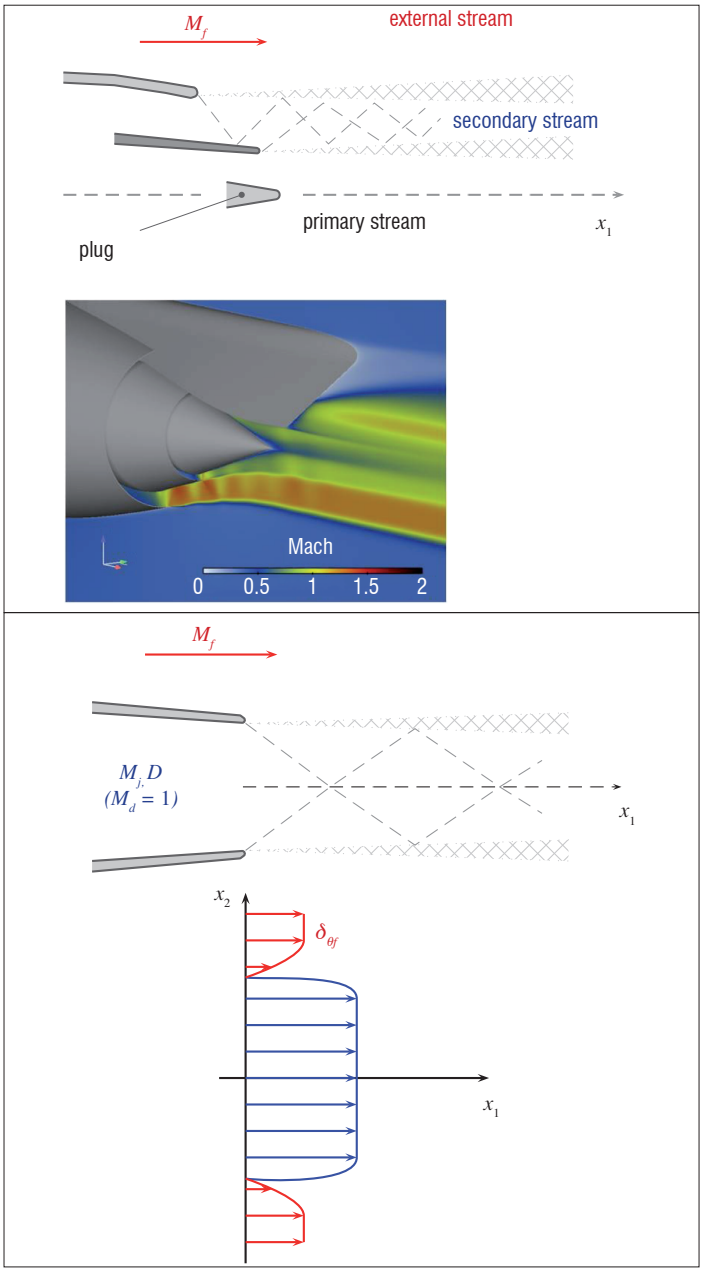

Figure 8 - Top – sketch of the exhaust of a commercial engine with a high bypass ratio, consisting of a central plug, the primary hot jet, the secondary cold underexpanded jet and the external stream characterized by its flight Mach number M_f. The Mach number field taken from a RANS simulation of a generic configuration is also shown [16]. The shock-cell structure in the secondary stream can be identified.
Bottom – sketch of the configuration to study flight effects in an anechoic wind-tunnel, with the shear layer between the supersonic stream and the external stream. The mean velocity profile induced at the nozzle exit is also shown, where $\delta_{\theta f}$ is the external boundary layer thickness.

Regarding velocity fluctuations, turbulence develops more slowly in space, since the mean velocity gradient is reduced, $\Delta u \sim u_j - u_f$, which can explain a small reduction of acoustic levels. In addition, the intrinsic time scale, that is, the integral time scale of turbulence in the convected frame, is found rather to be independent of M_f. Finally, examination of acoustic spectra [5] leads to the conclusions that the peak amplitude is practically not changed and that the overall amplitude is decreased by a few decibels.

The general formulation symbolized by expression (10) allows the inclusion of refraction effects in the BBSAN model of Morris and Miller [20]. This point is discussed in what follows. First, the vector Green functions can be analytically determined in the absence of a mean flow. The linearized Euler equations $\overline{\mathcal{L}}_i(\pi', \boldsymbol{u}') = f_i$ (with $f_0 = 0$) can indeed be reduced to a scalar wave equation $\partial_{tt}^2\pi' - c_\infty^2\nabla^2\pi' = -\nabla\bullet f$, for which the free space Green function is well-known. Therefore, it can be shown [16,20] that

$$\Pi^n(\boldsymbol{x},\boldsymbol{y},\omega) = \frac{ik_\infty}{4\pi c_\infty^2 x}\frac{x_n}{x}e^{-ik_\infty|\boldsymbol{x}-\boldsymbol{y}|} \qquad (11)$$

in the far field for $x \gg y$ and in the frequency domain with $k_\infty \equiv \omega / c_\infty$. The free space scalar Green function is however not known analytically in a more general context, but can be numerically determined by reformulating the problem for the adjoint Green function [35], for instance.

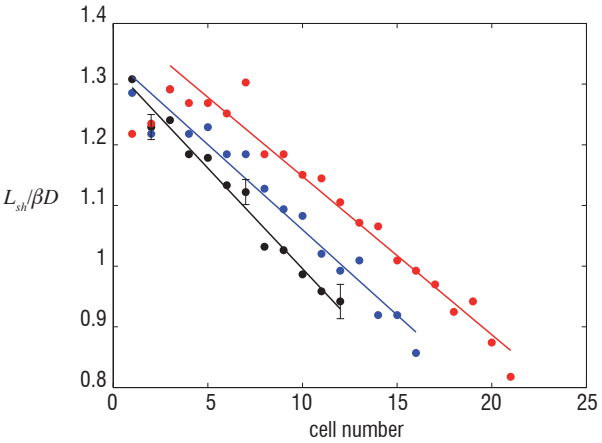

Figure 9 - Individual shock cell length L_{sh} normalized by βD as a function of the cell number and for three flight Mach numbers, • $M_f = 0$, • $M_f = 0.22$, • $M_f = 0.39$. The experimental data are obtained from Schlieren visualizations for the $M_j = 1.10$ jet [5,9].

An alternative approach is to account for mean flow effects using geometrical acoustics, since the associated assumptions are quite well satisfied by BBSAN [15,16]. Ray-tracing is an efficient and intuitive way to compute mean flow effects. The guiding idea consists in writing that each elementary volumetric source term $\delta W = W(\boldsymbol{y},\omega)\delta v$ of the BBSAN model radiates a fraction of this energy in a ray tube connecting the source $\boldsymbol{y}$ to the observer position $\boldsymbol{x}$, where $W(\boldsymbol{y},\omega)$ is the power spectral density per unit volume of the BBSAN source term. The conservation of energy along this ray tube permits the pressure fluctuation to be expressed at $\boldsymbol{x}$ and the scalar Green function to be identified. The link between this scalar Green function and the Π^n functions is more difficult to establish. In Henry et al. [15, 16], the mean flow is assumed to be parallel, in order to consider the third-order wave equation of Lilley [18] and to express this relation analytically [12]. Finally, the direct determination of eigen rays from the source at $\boldsymbol{y}$ to the observer at $\boldsymbol{x}$ is not very efficient. To compute BBSAN at a given position $\boldsymbol{x}$, an adjoint problem is considered by reversing the mean flow and by shooting from an observer position $\boldsymbol{x}$ to the source domain, as illustrated in figure 10.

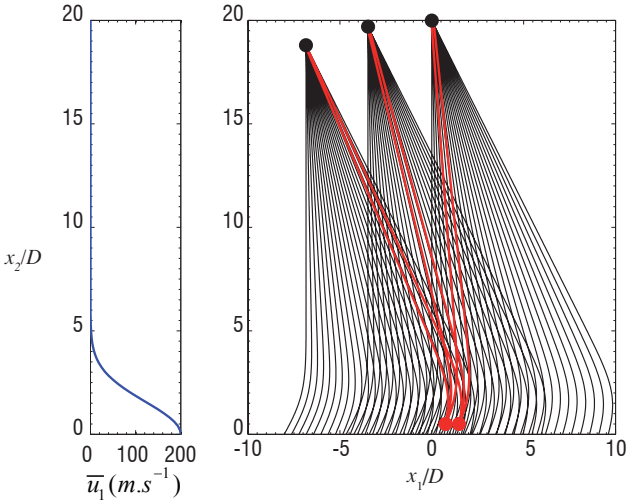

Figure 10 - Illustration of ray-tracing in the direct and adjoint problems, • observer positions, • source, — adjoint ray to the source domain at a given $\boldsymbol{x}$, — direct ray from the source $\boldsymbol{y}$ to the observer location $\boldsymbol{x}$.

Conclusion

Some properties of shock noise generated by underexpanded round jets issued from a convergent nozzle are briefly introduced in this paper. They are illustrated by experimental and numerical results from two recent studies [5, 16]. The work is aimed at developing a complete view of noise induced by a shock-cell structure, including flight effects. It can be emphasized that the characterization of flight effects on broadband shock-associated noise illustrates the good combination between experimental and numerical approaches, to complete the experimental test matrix for high subsonic flight Mach numbers, for instance. Identification of shock-cells contributing to screech and broadband shock-associated noise, characterization of the receptivity at the nozzle lip, or more quantitative analyzes of high-speed Schlieren images are topics that still require research efforts ■

Acknowledgment

This work was supported by the Labex CeLyA of Université de Lyon, operated by the French National Research Agency (ANR-10-LBX-0060/ ANR-11-IDEX-0007).

Acronyms

BBSAN	(BroadBand Shock-Associated Noise)
CFD	(Computational Fluid Dynamics)
LDV	(Laser Doppler Velocimetry)
NPR	(Nozzle Pressure Ratio)
PIV	(Particle Image Velocimetry)
RANS	(Reynolds-Averaged Navier-Stokes)

References

[1] M. ABBETT - *Mach Disk in Underexpanded Exhaust Plumes.* AIAA Journal, Vol. 9, N°. 3, 512-514, 1971.

[2] B. ANDRÉ, T. CASTELAIN, C. BAILLY - *Experimental Study of Flight Effects on Screech in Underexpanded Jets*. Phys. Fluids, Vol. 23, 126102, 1-14, 2011.

[3] B. ANDRÉ, T. CASTELAIN, C. BAILLY - *A Shock Tracking Procedure for Studying Screech Induced Oscillations*. AIAA Journal, Vol. 49, N°. 7, 1563-1566, 2011.

[4] B. ANDRÉ, T. CASTELAIN, C. BAILLY - *Shock Oscillations in a Supersonic Jet Exhibiting Antisymmetrical Screech*. AIAA Journal, vol. 50, N°. 9, 2017-2020, 2012.

[5] B. ANDRÉ - *Etude expérimentale de l'effet du vol sur le bruit de choc de jets supersoniques.* Ph.D. Thesis, ECL - N°. 2012-42, 2013.

[6] B. ANDRÉ, T. CASTELAIN, C. BAILLY - *Broadband Shock-associated Noise in Screeching and Non-Screeching Underexpanded Supersonic Jets*. AIAA Journal, Vol. 51, N°. 3, 665-673, 2013.

[7] B. ANDRÉ, T. CASTELAIN, C. BAILLY - *Experimental Investigation of Underexpanded Supersonic Jets.* To appear in Shock Waves, 2013.

[8] B. ANDRÉ, T. CASTELAIN, C. BAILLY - *Effect of a Tab on the Aerodynamical Development and Noise of an Underexpanded Supersonic Jet.* C. R.Méc., Acad. Sci. Paris, to appear, 2013.

[9] B. ANDRÉ, T. CASTELAIN, C. BAILLY - *Experimental Study of Flight Effects on Slightly Underexpanded Supersonic Jets.* 19th AIAA/CEAS Aeroacoustics Conference, AIAA Paper 2013-2079, 2013.

[10] B. ANDRÉ, T. CASTELAIN, C. BAILLY - *Investigation of the Mixing Layer in a Slightly Underexpanded Supersonic Jet by Particle Image Velocimetry*. Proceedings of the Eighth International Symposium on Turbulence and Shear Flow Phenomena (TSFP-8), 2013.

[11] C. BAILLY, P. LAFON, S. CANDEL - *Subsonic and Supersonic Jet Noise Predictions from Statistical Source Models*. AIAA Journal, Vol. 35, N°. 11, 1688-1696, 1997.

[12] C. BAILLY, C. BOGEY, S. CANDEL - *Modelling of sound Generation by Turbulent Reacting Flows*. International Journal of Aeroacoustics, Vol. 9, N°. 4-5, 461- 489, 2010.

[13] C. BOGEY, C. BAILLY - *An Analysis of the Correlations Between the Turbulent Flow and the Sound Pressure Field of Turbulent Jets*. J. Fluid Mech., Vol. 583, 71-97, 2007.

[14] M. HARPER-BOURNE, M.-J. FISHER - *The Noise from Shock Waves in Supersonic Jets*. Noise Mechanisms, N°. 131, 1973.

[15] C. HENRY, C. BAILLY, G. BODARD - *Statistical Modeling of BBSAN Including Refraction Effects*. 18th AIAA/CEAS Aeroacoustics Conference, AIAA Paper 2012-2163, 1-18, 2012.

[16] C. HENRY - *Prediction of Broadband Shock-associated Noise in Static and Flight Conditions*. Ph.D. Thesis, ECL - N°. 2012-60, 2012.

[17] J. HUBER, A. SYLLA, V. FLEURY, J. BULTÉ, K. BRITCHFORD, E. LAURENDEAU, D. LONG - *Understanding and Reduction of Cruise Jet Noise at Model and Full Scale*. 15th AIAA/CEAS Aeroacoustics Conference, AIAA Paper 2009-3382, 2009.

[18] G.-M. LILLEY - *The Generation and Radiation of Supersonic Jet Noise*. Vol. IV - Theory of Turbulence Generated Jet Noise, Noise Radiation from Upstream Sources, and Combustion Noise. Part II: Generation of Sound in a Mixing Region, AFAPL-TR-72-53, Vol. 4, 1972.

[19] P.-J.MORRIS - *A Note on the Effect of Forward Flight on Shock Spacing in Circular Jets*. J. Sound Vib., Vol. 121,N°. 1, 175-177, 1988.

[20] P.-J. MORRIS, A.-E. MILLER - *Prediction of Broadband Shock-associated Noise Using Reynolds-averaged Navier-Stokes Computational Fluid Dynamics.* AIAA Journal, Vol. 48, N°. 12, 2931-2944, 2010.

[21] P.-J. MORRIS, F. FARASSAT - *Acoustic Analogy and Alternative Theories for Jet Noise Predictions.* AIAA Journal, Vol. 40, N°. 4, 671-680, 2002.

[22] T.D. NORUM - *Screech Suppression in Supersonic Jets*. AIAA Journal, Vol. 21, N°. 2, 235-240, 1983.

[23] J. PANDA - *An Experimental Investigation of Screech Noise Generation.* J. Fluid Mech., Vol. 378, 71-96, 1999.

[24] S. PAO, J. SEINER - *Shock Associated Noise in Supersonic Jets.* AIAA Journal, Vol. 21, N°. 5, 687-693, 1983.

[25] A. POWELL - *On the Noise Emanating from a Two Dimensional Jet Above the Critical Pressure.* Aeronautical Quarterly, Vol. 4, 103-122, 1953.

[26] A. POWELL - *On the Mechanism of Choked Jet Noise*. Proc. Phys. Soc. London, Sect. B66, 1039-1057, 1953.

[27] A. POWELL, Y. UMEDA, R. ISHII - *The Screech of Round Jets, Revisited.* 13th AIAA Aeroacoustics Conference, AIAA Paper 90-3980, 1990.

[28] A. POWELL - *On Prandtl's Formulas for Supersonic Jet Cell Length*. Int. Journal of Aeroacoustics, Vol. 9, N°. 1 & 2, 207-236, 2010.

[29] G. RAMAN - *Advances in Understanding Supersonic Jet Screech: Review and Perspective.* Prog. Aerospace Sci., Vol. 34, 45-106, 1998.

[30] J.-M. SEINER - *Advances in High Speed Jet Aeroacoustics*. 9th Aeroacoustics Conference, AIAA Paper 84-2275, 1984.

[31] T. SUZUKI, S. LELE - *Shock Leakage Through an Unsteady Vortex-laden Mixing Layer: Application to Screech Jet*. J. Fluid Mech., Vol. 490, 139-167, 2003.

[32] C.-K.-W. TAM, H.-K. TANNA - *Shock Associated Noise of Supersonic Jets from Convergent-divergent Nozzles.* J. Sound Vib., Vol. 81, N°. 3, 337-358, 1982.

[33] C.-K.-W. TAM, J.-A. JACKSON, J.-M. SEINER - *A Multiple-scales Model of the Shock-cell Structure of Imperfectly Expanded Supersonic Jets*. J. Fluid Mech., Vol. 153, 123-149, 1985.

[34] C.-K.-W. TAM - *Supersonic Jet Noise*. Annu. Rev. Fluid Mech., Vol. 27, 17-43, 1995.

[35] C.-K.-W. TAM, L. AURIAULT - *Mean Flow Refraction Effects on Sound Radiated from Localized Sources in a Jet*. J. Fluid Mech., Vol. 370, 149-174, 1998.

[36] C.-K.-W. TAM, N.-N.PASTOUCHENKO, K. VISWANATHAN - *Broadband Shock-cell Noise from Dual Stream Jets*, J. Sound Vib., Vol. 324, N°. 3-5, 861-891, 2009.

AUTHORS

Christophe Bailly. Professor at Ecole Centrale de Lyon (ECL), associated with Institut Universitaire de France (2007-2012). Background: PhD from Ecole Centrale Paris in 1994, joined Centre Acoustique of the Laboratoire de Mécanique des Fluides et d'Acoustique (LMFA UMR CNRS 5509) at ECL in 1995.

Benoît André. CFD engineer at ebm-papst St. Georgen (Germany). Background: Graduated from Ecole des Ponts ParisTech (2009), PhD from Ecole Centrale de Lyon (2012).

Thomas Castelain. Assistant Professor at Université Lyon I. Background: PhD from Ecole Centrale de Lyon (2006). Main interests include subsonic and supersonic jet noise, microjets for noise reduction, experimental flow control.

Cyprien Henry. Rotor dynamics engineer at Snecma. Background: PhD from Ecole Centrale de Lyon (2012) in collaboration with Snecma, Master of Sciences from ECL in 2009 (in Aeronautics).

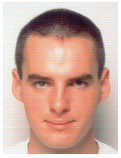

Guillaume Bodard. Engineer in Acoustics at Snecma. Background: Graduated from ENSMA (Ecole Nationale Supérieure de Mécanique et d'Aérotechnique de Poitiers, 2006), PhD fromEcole Centrale de Lyon (2009).

Mauro Porta. Jet noise specialist at Airbus Operations SAS Toulouse. Degree in aerospace engineering at Politecnico di Milano, 2003. PhD on Large Eddy Simulation for combustion chambers at INP Toulouse - Cerfacs, 2007.